Title

Pharmacological Reprogramming of Fibroblasts into Neural Stem Cells by Signaling-Directed Transcriptional Activation

Journal

Cell Stem Cell, 18(5)

ISSN

1934-5909

Authors

Zhang, Mingliang
Lin, Yuan-Hung
Sun, Yujiao Jennifer
et al.

Publication Date

2016-05-01

DOI

10.1016/j.stem.2016.03.020

Peer reviewed

HHS Public Access

Author manuscript

Cell Stem Cell. Author manuscript; available in PMC 2017 May 05.

Published in final edited form as:

Cell Stem Cell. 2016 May 5; 18(5): 653–667. doi:10.1016/j.stem.2016.03.020.

Pharmacological Reprogramming of Fibroblasts into Neural Stem Cells by Signaling-Directed Transcriptional Activation

Mingliang Zhang[1,2,9], **Yuan-Hung Lin**[3,4], **Yujiao Jennifer Sun**[7], **Saiyong Zhu**[1,2,9,10], **Jiashun Zheng**[8], **Kai Liu**[1,2,9], **Nan Cao**[1,2,9], **Ke Li**[1,2,9], **Yadong Huang**[2,3,5,6], and **Sheng Ding**[1,2,9,*]

[1]Gladstone Institute of Cardiovascular Disease, San Francisco, CA 94158, USA

[2]Roddenberry Center for Stem Cell Biology and Medicine, Gladstone Institutes, San Francisco, CA 94158, USA

[3]Gladstone Institute of Neurological Disease, San Francisco, CA 94158, USA

[4]Neuroscience Graduate Program, University of California, San Francisco, San Francisco, CA 94158, USA

[5]Department of Neurology, University of California, San Francisco, San Francisco, CA 94158, USA

[6]Department of Pathology, University of California, San Francisco, San Francisco, CA 94158, USA

[7]Department of Physiology, University of California, San Francisco, San Francisco, CA 94158, USA

[8]Department of Biochemistry and Biophysics, University of California, San Francisco, San Francisco, CA 94158, USA

[9]Department of Pharmaceutical Chemistry, University of California, San Francisco, San Francisco, CA 94158, USA

SUMMARY

Cellular reprogramming using chemically defined conditions, without genetic manipulation, is a promising approach for generating clinically relevant cell types for regenerative medicine and drug

[*]Correspondence: sheng.ding@gladstone.ucsf.edu (S.D.).

[10]Present address: Life Sciences Institute, Zhejiang University, Hangzhou, Zhejiang 310058, China

ACCESSION NUMBERS

The accession numbers for the RNA-seq and ChIP-seq data reported in this study are GEO: GSE78938 and GSE78978.

SUPPLEMENTAL INFORMATION

Supplemental Information includes Supplemental Figures S1–S6 and legends, Supplemental Tables S1–S6, and Supplemental Experimental Procedures.

AUTHOR CONTRIBITIONS

M.Z. and S.D. designed experiments and wrote manuscript. M.Z. performed experiments. Y.H.L. and Y.H. designed and performed *in vivo* injection and imaging. Y.S. performed electrophysiological experiments. M.Z. and K.L. analyzed RNA-seq data. J.Z. processed and analyzed ChIP-seq data. S.Z. and N.C. helped to design experiments and edited manuscript. K.L. assisted in reagents. S.D. supervised the study.

discovery. However, small molecule approaches for inducing lineage-specific stem cells from somatic cells across lineage boundaries have been challenging. Here, we report highly efficient reprogramming of mouse fibroblasts into induced neural stem cell-like cells (ciNSLCs) using a cocktail of nine components (M9). The resulting ciNSLCs closely resemble primary neural stem cells molecularly and functionally. Transcriptome analysis revealed that M9 induces a gradual and specific conversion of fibroblasts towards a neural fate. During reprogramming specific transcription factors such as Elk1 and Gli2 that are downstream of M9-induced signaling pathways bind and activate endogenous master neural genes to specify neural identity. Our study provides an effective chemical approach for generating neural stem cells from mouse fibroblasts, and reveals mechanistic insights into underlying reprogramming processes.

INTRODUCTION

Generation of expandable neural stem cells (NSCs) from fibroblasts with full developmental potential represents a promising therapeutic approach for treating neurodegenerative diseases or injuries. By ectopic expression of NSC-specific transcription factors (TFs) (Han et al., 2012; Lujan et al., 2012), or transient expression of pluripotency factors (Kim et al., 2011; Lu et al., 2013; Thier et al., 2012; Wang et al., 2013; Zhu et al., 2014), combined with the neural specification signals, mouse and human fibroblasts can be successfully induced into expandable NSCs. Those exogenous pioneer TFs overexpressed in the fibroblasts directly recognize specific loci across the genome and recruit and orchestrate with other transcriptional regulators to remodel the epigenome of the host cells, and eventually establish the NSC identity. This reprogramming strategy may ultimately provide an avenue to patient-specific cell-based or *in situ* regenerative therapy. Compared to the genetic approach, small molecule-based chemical strategies may have several important advantages (Xu et al., 2013; Zhang et al., 2014). Small molecules are relatively easy to apply, optimize and manufacture, and they can be more readily developed into conventional pharmaceuticals. Unlike the reprogramming mediated by pioneer TFs, chemical-induced cellular reprogramming represents a different process. Mechanistically, small molecules interact with and modulate endogenously pre-existing proteins of the starting cell type (e.g., fibroblasts), and indirectly and ultimately gain and establish target cell type specificity. Therefore, chemical reprogramming would provide a novel approach and process to investigate the underlying mechanism of cell fate conversion.

A previous study reported a chemical cocktail that induced fibroblasts into neural progenitor cells under hypoxia condition (Cheng et al., 2014). Not only mechanism underlying such reprogramming remains elusive, but also most of previous studies on NSC reprogramming started with undefined mouse embryonic fibroblasts (MEFs) (Cheng et al., 2014; Han et al., 2012; Kim et al., 2011; Ring et al., 2012; Thier et al., 2012). MEFs are an inherently heterogeneous population containing non-fibroblast precursor cell types that may be specified into neural lineage via processes other than *bona fide* reprogramming. To unambiguously define the origin of cells that are reprogrammed into NSCs, genetic lineage tracing of the starting fibroblasts would be required (Cassady et al., 2014), especially in conditions that use combinations of small molecules given the indirect induction mechanisms of reprogramming and differentiation.

To this end, using purified MEFs that were genetically labeled with tdTomato via a validated fibroblast-specific Fsp1-Cre lineage tracing system, we rationally screened combinations of small molecules and identified a specific combination of nine components (M9) that could efficiently convert the fibroblasts into chemical-induced NSC-like cells (ciNSLCs). The resulting ciNSLC are tripotent and can robustly differentiate into three neural lineages, including astrocytes, oligodendrocytes and functional neurons. Moreover, ciNSLC have very similar gene expression profile and self-renewal ability comparing to primary NSCs. Initial mechanistic studies further uncovered how the fibroblasts are gradually and specifically reprogrammed toward the NSC fate via activation of endogenous *Sox2*. Our study not only provides a completely chemically defined approach to generating NSCs from fibroblasts, but also provides molecular insights into the chemical-induced neural reprogramming process.

RESULTS

Defining Starting Fibroblasts via Lineage Tracing

Because primary MEFs contain heterogeneous populations of non-fibroblast precursor cells, it is essential to unambiguously define the origin/identity of the starting fibroblasts for chemical-based reprogramming with a genetic lineage tracing strategy. Fibroblast-specific protein 1 (Fsp1, also known as S100α4) has been shown and validated as a specific marker for fibroblasts, and Fsp1-Cre has been used to lineage-trace fibroblast origin (Qian et al., 2012). Consequently, cells were isolated from transgenic mice carrying Fsp1-Cre/ROSA26^{tdTomato} at E13.5, and the fibroblast population was permanently marked with tdTomato expression. Besides removing neural tissues from the MEF preparations, we performed FACS sorting to collect the tdTomato^{+}/p75^{-} population to exclude any neural crest progenitors (hereafter named tdMEF, Figure 1A and S1A). These tdMEFs were negative for typical NSC markers, including Sox2, Pax6 and Olig2 (Figure S1B and Table S1). They showed very low-level expression of Nestin, but the pattern was quite different from that of primary NSCs (Figure S1B). In addition, tdMEFs were negative for glial fibrillary acidic protein (GFAP) and neural/glial antigen 2 (NG2), markers for astrocytes/radial glia cells and oligodendrocyte progenitor cells, respectively, that have the potential to become NSCs (Figure S1B) (Doetsch et al., 1999; Kondo and Raff, 2000). We confirmed the absence of several neural gene transcripts, including *Pax6, Sox2, Hes5, Ascl1, Gfap* and *Olig2*, in tdMEFs by RT-PCR (Figure S1C and Table S2). To further confirm the absence of neuron-producing cells, tdMEFs were cultured under extended neuronal differentiation condition. No Tuj1^{+} neurons were detected from 10^5 starting tdMEFs after a 15-day differentiation (data not shown). Consequently, these tdMEFs were established as suitable starting cells for chemical-based neural reprogramming studies.

Identification of Chemically Defined Condition to Reprogram Fibroblasts into Neural Stem Cells

We hypothesized that treating cells with a combination of small molecules that target epigenetic modifications and modulate neuro-developmental signaling would induce the neural transcriptional program in fibroblasts. To begin a combinatorial chemical screening, LDN193189 (LDN, an inhibitor of BMP type I receptor ALK2/3) and A83-01 (A83, an inhibitor of TGF-β type I receptor ALK4/5/7), which inhibit mesoderm and endoderm

specification (Chambers et al., 2009; Smith et al., 2008; Smith and Harland, 1992), and CHIR99021 (CHIR, a GSK3 inhibitor) and basic fibroblasts growth factor (bFGF), which favor neural development (Gritti et al., 1996; Li et al., 2011), were combined as a neural induction basal condition in a chemically defined medium, on top of which other individual small molecules were screened for induction of neural reprogramming of tdMEFs. Briefly, tdMEFs were plated at 15,000 cells per well in a 24-well plate. After overnight culture, tdMEFs were treated in neural reprogramming basal medium with addition of individual small molecules from a focused chemical collection, including epigenetic modifiers, metabolism regulators, and signaling modulators. Ten days post-treatment, cells were fixed, immuno-stained, and analyzed for co-expression of Sox2 and Nestin, two typical NSC markers (Figure 1A and B). From the primary screening, Hh-Ag 1.5 (Hh, a potent Smo agonist) and retinoic acid (RA) were found to induce the generation of 3.68 % and 1.26 % $Sox2^+/Nestin^+$ cells, respectively, while DMSO treated control wells had no $Sox2^+/Nestin^+$ cells. These two chemicals were subsequently included into the basal condition, and small molecules were screened again on top of the six-molecule condition for ones that could further improve the neural induction efficiency. Notably, RG108 (RG, a DNA methyltransferase inhibitor), Parnate (Par, a histone demethylase inhibitor), and SMER28 (SR, an autophagy modulator) further enhanced the generation of $Sox2^+/Nestin^+$ cells. Particularly, addition of SR improved the conversion efficiency for adult tail-tip fibroblasts. These three small molecules were included into the neural induction cocktail, resulting in a nine-component combination of CHIR, LDN, A83, RA, Hh, RG, Par, SR and bFGF (Table S3), that robustly induced $Sox2^+/Nestin^+$ cells at percentage of ~24.20–30.04 % (Figure 1F). To identify indispensible molecules, each component was individually removed from the cocktail and the neural reprogramming efficiency was evaluated. Removing any of the nine components significantly reduced the reprogramming efficiency (Figure S1D). This combination of nine components (named as M9 hereafter) was used in subsequent assays after optimization of dosage (Figure S1E).

To characterize the reprogramming process, it was observed that the M9-treated tdMEFs morphologically underwent a characteristic mesenchymal-to-epithelial transition (MET) and small cell colonies gradually emerged towards day 6 (Figure S1F). These METed colonies were positive for alkaline phosphatase (ALP, Figure S1G). Remarkably, during day 6 to day 10, induction of the Sox2, the master transcriptional factor for NSCs, was observed in cell colonies. By day 10, the percentage of $Sox2^+/Nestin^+$ cells reached approximately 25 % (Figure 1B and F). Semi-quantitative RT-PCR confirmed the expression of other NSC genes, including *Pax6*, *Sox2*, *Ascl1*, and *Olig2*, in this population (Figure S1H).

Further examination of the M9-induced neural reprogramming process revealed that generation of these METed cell colonies would only require as short as 6 days, while expression of NSC genes in these colonies could not be maintained in the absence of M9, indicating an unstable/incomplete transition status by day 6 (data not shown). However, it was found that 10-day induction is sufficient to induce the stable expression of NSC genes (Figure 1B and C). After passaging, the whole population became morphologically homogeneous (Figure S2A). The homogeneity was further examined by analyzing the expression of Sox2, Nestin, and an additional NSC marker Pax6. By immunostaining, we found the percentage of cells co-expressing Sox2 and Nestin, Pax6 and Nestin, or Sox2 and

Pax6, was about 87.46 %, 92.12 %, and 79.95 % at passage 2, and 97.62 %, 94.39 % and 93.36 % at passage 12, respectively. Notably, all these $Sox2^+/Nestin^+$ cells also expressed tdTomato, demonstrating a conversion from fibroblasts (Figure 1B and C).

Characterization of M9-Induced ciNSLCs

To further characterize M9-induced $tdTomato^+/Sox2^+/Nestin^+$ cells, they were serially propagated in conventional NSC expansion medium containing bFGF and epidermal growth factor (EGF) (Conti et al., 2005; Pollard et al., 2006). These cells were highly proliferative, as 73.53 % ± 4.10 % of the cells showed incorporation of BrdU (Figure 1C). They were able to form neurospheres in suspension culture over at least 10 passages (Figure S2A). These cells showed exponential growth in a quantitative manner, similar to primary neural progenitor cells (pri-NPC) and NSC line SCR029 (Figure S2B). FACS analysis with propidium iodide staining showed that the cell cycle distribution (G0/G1, S, and G2/M phases) was 41.30 %, 8.11 %, and 41.10 % for passage 2, and 57.30 %, 11.50 % and 30.60 % for passage 12, similar cell cycle profiles with that of pri-NPC and SCR029 (Figure S2C). Morphologically, these cells maintained a non-polarized homogeneous population in monolayer culture, and did not form polarized rosette-structure (Figure 1C and Figure S2A). These cells expressed multiple central nervous system NSC markers, including Sox2, Nestin, Pax6, Olig2 and N-cadherin (Figure 1C, 1D and Table S4). The expression of these genes in independent lines was comparable to those in pri-NPCs and SCR029 (Figure 1D). By immunostaining or RNA-seq, we could not detect the expression of Dach1 and PLZF (also known as Zbtb16) (Elkabetz et al., 2008), but some radial glia-like cell markers, such as Glast (also known as Slc1a3) and BLBP (also known as Fabp7) (Table S5), indicating that these cells may resemble bFGF/EGF-adopted post-rosette-stage neural stem cells (Conti et al., 2005; Glaser et al., 2007; Koch et al., 2009; Pollard et al., 2006). Transcriptome analysis revealed that these cells closely resembled mouse NSCs, but were distinct from tdMEFs (Figure 1E). Those fibroblast-originated, highly proliferative, and self-renewable Sox2/Nestin double-positive cells are thereafter referred to as chemical-induced neural stem cell-like cells (ciNSLCs).

In addition to reproducible results with different batches of tdMEFs (n=4), MEFs with different genetic backgrounds were also tested with the M9 condition. Ten days after M9 treatment, the percentage of $Sox2^+/Nestin^+$ cells was about 16.40 % and 27.95 % for MEFs of 129×C57BL/6, or 129 background, respectively (Figure 1F). Furthermore, M9 could induce Fsp1-Cre/$ROSA26^{tdTomato}$-traced mouse tail-tip fibroblasts (tdTTF) into ciNSLCs, albeit at a lower reprogramming efficiency (about 0.6–2.9 %, Figure 1F). The tdTTF-derived ciNSLCs resemble pri-NPCs, as they have comparable expression of multiple NSC markers, as evidenced by qRT-PCR (Figure 1D) and immunostaining (Figure S3A), similar proliferation rate (Figure S2B), and the ability to differentiate into mature neurons (Figure S3B).

To determine if $tdTomato^+$ cells exhibited any preferential response to M9 treatment, we sorted Fsp1-Cre/$ROSA26^{tdTomato}$ MEFs by FACS into $p75^-/tdTomato^+$ and $p75^-/tdTomato^-$ populations, and treated them with M9 condition. About 26.7 % of $tdTomato^+$ cells and 31.0 % of $tdTomato^-$ cells became $Sox2^+/Nestin^+$ ciNSLCs 10 days after M9 treatment,

demonstrating a comparable efficiency (Figure S2D). These results collectively demonstrate that M9 cocktail has a robust and general effect on reprogramming fibroblasts into ciNSLCs.

M9-Induced ciNSLCs Are Tripotent *in vitro* and *in vivo*

To characterize the differentiation potential of expanded ciNSLCs, they were first cultured under spontaneous differentiation condition without bFGF and EGF. By immunostaining, ciNSLCs gave rise to approximately 67.9 % $Tuj1^+$ neurons and 16.5 % $GFAP^+$ astrocytes at passage 5, and this differentiation potential was well maintained during prolonged culture (passage 10, Figure 2H).

To examine the neuron differentiation *in vitro* (Kim et al., 2011), we observed $tdTomato^+$ cells with immature neuronal morphology as early as day 3 (Figure S4A). Upon further differentiation, mature neurons with elaborate processes that expressed a panel of typical neuronal markers, including Tuj1, Map2, NeuN, and Synapsin I, were readily detected at day 10 onwards (Figure 2A–C). Subsequent analysis revealed that most of the neurons were $vGlut1^+$, indicating an excitatory glutamatergic phenotype, while ~ 8.6–14.7 % were $GABA^+$ inhibitory neurons (Figure 2D, E and I).

To more rigorously characterize these differentiated neurons, we examined their electrophysiological properties. As expected, they generated repetitive trains of action potentials elicited by depolarizing the membrane in the current-clamp mode (8 out of 11, Figure 3A). In addition, the inactivating inwards and persistent outwards currents were observed in the voltage-clamp mode, which could be blocked by tetrodotoxin (TTX, 3 out of 3) or tetraethylammonium (TEA, 3 out of 3), respectively, indicating the presence of functional sodium- or potassium- channels (Figure 3B and C). Furthermore, the ciNSLC-derived neurons exhibited strong spontaneous synaptic network activities (4 out of 11, Figure 3D), suggesting the formation of functional synapses, consistent with Synapsin I expression at the synaptic puncta along dendrites (Figure 2C). Moreover, these neurons responded to direct activation of excitatory (glutamate, 3 out of 3, Figure 3E) or inhibitory neurotransmitter receptors (GABA, 2 out of 5, Figure 3F), and exhibited postsynaptic currents. These results demonstrated that ciNSLCs could generate functional neurons *in vitro*.

In addition to neuronal differentiation, ciNSLC can differentiate into $O4^+$ oligodendrocytes with typical multi-branching morphology after treatment with T3 (Figure 2F and Figure S4B) (Glaser et al., 2007; Najm et al., 2013). Importantly, those differentiated oligodendrocytes expressed myelin basic protein (MBP, Figure 2F), and other defining markers of mature oligodendrocytes, including myelin-associated glycoprotein (MAG) and myelin oligodendrocyte glycoprotein (MOG) (Figure S4B), and can myelinate the axons *in vitro* (Figure S4C). ciNSLC can also generate characteristic GFAP-, and S100β-positive astrocytes when treated with BMP4 (Figure 2G). Quantitative RT-PCR revealed the upregulation of glial genes, including *Gfap* for astrocytes, and *Mbp and Plp1* for oligodendrocytes, upon directed differentiation (Figure S4D). Thus, the expanded ciNSLCs are tripotent and can robustly generate neurons, astrocytes, and oligodendrocytes *in vitro*.

To determine ciNSLC's differentiation potential *in vivo*, they were microinjected into the cortices of postnatal mouse pups (n=6), and their survival and differentiation were evaluated 2–4 weeks after injection. Remarkably, tdTomato-marked ciNSLC progeny survived in the cortex of all mice we analyzed. These ciNSLCs efficiently differentiated into NeuN-positive mature neurons, Olig2-positive oligodendrocytes, and GFAP-positive astrocytes (Figure 3G). No tumor was found 4 weeks post-injection (data not shown). This *in vivo* differentiation potential of ciNSLCs was validated by two independent ciNSLC lines. Taken together, the expanded ciNSLCs resemble primary NSCs by their marker expression and abilities to self-renew and differentiate *in vitro* and *in vivo*.

Characterization of Regional Property of Stable ciNSLC

To determine the regional identity of ciNSLC, the expression of regional markers along the anterior-posterior and dorsal-ventral axes of neural tube were analyzed. The early-passage ciNSLC (passage 2) stained positive for the forebrain marker Foxg1, but did not express the midbrain marker En1, and hindbrain marker Hoxa2 and/or posterior marker Hoxb4 (Figure 4A and C). However, the anterior identity was lost in late-passage ciNSLCs (passage 12), which acquired posterior identity and stained positive for Hoxb4 (Figure 4B). We confirmed this transition by qRT-PCR or RNA-seq. In contrast to passage 2, which exhibited high expression of the forebrain gene *Foxg1*, ciNSLCs at passage 12 showed no expression of *Foxg1* and *En1*, but predominantly expressed the hindbrain and spinal cord genes, including *Hoxa2*, *Hoxa3*, *Hoxa5*, and *Hoxb4*, indicating a posterior regionalization of stable ciNSLC (Figure 4C and Table S5). Along dorsal-ventral axis, stable ciNSLCs showed high expression of ventral genes *Olig2* and *Nkx2.2*, whereas no or low expression of other ventral and dorsal genes, such as *Pax3* and *Pax7*, respectively (Figure 4C and Table S5). Therefore, the stable ciNSLCs are mostly compatible with a posterior ventral fate.

To confirm this regional property, we found that ciNSLCs at passage 12 exhibited propensity to differentiate into choline acetyltransferase (ChAT)-, and Islet1-positive neurons after 15 day differentiation in the presence of 10 ng/ml BDNF, 20 ng/ml GDNF, 10 ng/ml NT3, 2 μM db-cAMP and 200 μM ascorbic acid (Figure S4E). We did not observe neurons that stained positive for tyrosine hydroxylase or serontonin, for both early- and late-passage ciNSLCs (data not shown). When these stable ciNSLCs were subjected to an "induced" differentiation protocol (pre-patterned with 1 μM RA and 200 ng/ml Shh for 5 days, and then cultured in presence of 10 ng/ml BDNF, 20 ng/ml GDNF, 10 ng/ml NT3, 2 μM db-cAMP and 200 μm ascorbic acid for 7–10 days), they became further specified towards a ventral fate with high expression of Olig2 and Nkx2.2 (Figure 4D). Further differentiation of these RA and Shh patterned ciNSLCs showed that 61.90 % ± 4.85 %, and 64.12 % ± 2.80 % of cells are double-positive for Map2 with ChAT (Figure 4E), and Islet1 (Figure 4F), respectively, indicating a ventral fate motor neurons. In contrast, treating ciNSLCs with Fgf8 (100 ng/ml) and Shh (200 ng/ml) failed to induce expression of midbrain marker En1 (data not show), consistent with the specified posterior ventral regional identity of stable ciNSLCs.

Molecular Roadmap of M9-Induced Neural Reprogramming

To monitor the activation of endogenous neural fate regulators, we initially examined Sox2 expression by immunostaining (Figure S5A). Expression of Sox2 in individual cells was

observed as early as day 4 upon M9 treatment (1.29 % of total cells), and that number increased significantly in METed small colonies around day 8 (7.32 %). By day 10, robust expression of Sox2 was detected in cells within large and flat colonies (24.20 %). Upon passaging and expansion, most cells stained positive for Sox2 (> 90 % in passage 2). In addition to Sox2, similar kinetics of gene activation for other neural genes, such as *Pax6, Olig2, Hes5* and *Ascl1*, was also detected by qRT-PCR and RNA-seq (Figure 5A and S5B), indicating that M9 effectively activated the intrinsic neural program.

To elucidate the reprogramming route, transcriptome over neural induction process was analyzed by RNA-seq (Figure 5B). Principle components analysis revealed that all intermediates, upon M9 treatment, were distinct from starting tdMEFs (D0), indicating M9 treatment led to dramatic transcriptional changes (Figure 5C). By analyzing the differentially expressed genes, a gradual transition from fibroblasts towards NSCs was observed (Figure 5B). The genes highly expressed in both ciNSLCs and control NSCs fell into categories of neural development related biological processes (Figure 5B and Figure S6A), confirmed an acquisition of NSC identity, whereas genes that were downregulated from day 4 onwards were involved in fibroblast function, such as extracellular matrix/structure organization and cell adhesion (Figure 5B). Interestingly, we found that genes showing transient activation in reprogramming intermediates were involved in inflammatory responses and wound healing, as well as epithelium development (Figure 5B). These findings are supported by previous studies showing that the activation of innate immunity and the MET process are critical for efficient reprogramming (Lee et al., 2012; Li et al., 2010). To confirm this fibroblast-to-neural stem cell transition, we checked the expression of 19 fibroblast- and 32 neural stem cell-related genes (Figure 5D). Fibroblasts genes, such as *S100α4*, and *Periostin*, were significantly downregulated; whereas a panel of NSC genes was gradually upregulated during the ciNSLC induction process.

To examine the reprogramming specificity towards neural lineage, we analyzed the expression of genes in non-neural lineage upon M9 treatment. Remarkably, except for the gradual acquisition of neural gene expression (Figure S6B), we could not detect the transcripts of other lineage-specific master genes, such as *Nanog, Oct4* and *Rex1* (pluripotency), *Brachyury* and *Mesp1* (mesoderm), *Sox17* and *Foxa2* (endoderm), and *Sall4*, *Gata4* and *Sox7* (extra-embryonic endoderm), suggesting a specific activation of neural program (Table S5). To confirm this specificity, we analyzed the expression of a cohort of genes that are under the gene ontology (GO) terms of ectoderm, mesoderm, and endoderm development, fibroblasts, and stem cell maintenance, respectively, at day 4 after M9 treatment. Consistently, the transcriptional activation was predominantly towards ectoderm, rather than the other lineages (Figure 5E).

To investigate how transcriptional rewiring was achieved at the epigenetic level, we tracked histone modifications, including H3K4me1, H3K4me3, H3K27me3, and H3K27Ac, at −2kb to 3kb from gene transcriptional starting site by ChIP-seq upon M9 treatment. As no dramatic change was observed globally, gain of the active mark H3K4me3 and loss of the repressive mark H3K27me3 occurred most at the early stage (D0 to D4 transition), indicating a global chromatin remodeling responsive to M9 treatment (Figure S6C). To validate the neural reprogramming, a dramatic increase of H3K4me3 was observed at

promoter of genes involving in ectoderm development upon M9 treatment, concomitantly with the reduction of H3K27me3, indicating a global induction of neural genes (Figure 5F and G). In contrast, the promoter of fibroblast-associated genes showed a gradual loss of H3K4me3 and gain of H3K27me3, which collectively supported a fibroblast-to-neural fate transition (Figure 5F and G). This transition was confirmed by monitoring 32 NSC-enriched gene loci (Figure 5H). Among these genes, a dramatic epigenetic activation at *Sox2* genome loci was detected, with gradual gain of H3K4me3 and H3K27Ac, and loss of H3K27me3 (Figure 5I), which was validated by ChIP-qPCR (Figure 5J–L). This chromatin landscape was firmly established in ciNSLCs and resembled those of NSCs (Figure 5F–L), supporting a neural reprogramming.

Transcriptional Activation downstream of bFGF and Shh Dictates Neural Reprogramming

While we found that removing any of the nine molecules significantly reduced the reprogramming efficiency, omitting bFGF or Hh-Ag 1.5 affected the ciNSLC induction most (Figure S1D). To explore the function of bFGF and Hh-Ag 1.5 on reprogramming, we examined how inhibiting their downstream signaling would affect ciNSLC induction. To dissect the function of bFGF signaling, the major downstream pathways triggered by bFGF, including mitogen-activated protein kinase (MAPK) pathways, and phosphatidylinositol 3-kinase (PI3K) pathway, were individually blocked with specific small molecule inhibitors, PD0325901 (a MEK inhibitor), SP600125 (a JNK inhibitor), SB203580 (a p38 inhibitor), or LY294002 (a PI3K inhibitor), under the M9 induction condition (Figure 6A). With the inhibitor, the reprogramming efficiency was dramatically reduced about 9-fold by PD0325901, 6-fold by SP600125, 5-fold by SB203580, and 4-fold by LY294002, suggesting different contributions of bFGF downstream signaling pathways to its reprogramming inducing effect. Consistently, we found that inhibiting Sonic Hedgehog (Shh) pathway with LDE-225 (a Smo antagonist) also significantly reduced the reprogramming efficiency by about 6-fold (Figure 6B).

Given the functional importance of bFGF and Hh-Ag 1.5 in ciNSLC reprogramming, we hypothesized that the immediate downstream TFs of bFGF and Shh pathways may directly participate in transcriptional activation of endogenous NSC master genes. Elk1 and Gli2 are the major direct TFs downstream of bFGF pathway and Shh pathway, respectively, and have been implicated in neurodevelopment (Besnard et al., 2011; Lai et al., 2003; Machold et al., 2003; Takanaga et al., 2009). To explore whether these factors are activated by M9 during neural reprogramming, we first checked their expression. By qRT-PCR, we found that they were both induced by M9 at transcriptional level (Figure 6C and D). Furthermore, we analyzed their activation at biochemical level. Elk1 is known to be phosphorylated (Cruzalegui et al., 1999), and the phosphorylated form, in turn, may serve as an active transcription regulator (Babu et al., 2000; Yang et al., 1999). Although the expression of Elk1 in the presence of M9 was just slightly increased compared to control (DMSO), we found that the phosphorylation of Elk1 protein (p-Elk1) was dramatically induced as revealed by immunostaining and Western blot analysis (Figure 6E–G). This result demonstrates that Elk1 is activated by M9. It has been reported that the full length Gli2 acts as transcription activator, which was maintained in response to Shh signal probably through protecting Gli2 from degradation (Pan et al., 2006). Immunostaining recognized both the full

length and proteolytic forms of Gli2 (Figure 6H). By Western blot, we found that full length Gli2 was well maintained only in the presence of M9 (Figure 6I and J). Therefore, M9 stabilizes Gli2, which, in turn, serves as transcription activator to induce downstream gene expression. Collectively, these results revealed that M9 activates both transcription factors.

To establish whether Elk1 and Gli2 directly participating in activating neural program, we examined how knock-down of them individually with shRNA affected ciNSLC induction by M9. Consistent with the aforementioned results (Figure 6A, B and S1D), knocking down either *Elk1* or *Gli2* dramatically reduced the reprogramming efficiency, confirming that they positively regulate reprogramming (Figure 6K and L). Importantly, knocking down these genes at the early stage (D0 and D4 versus D8) affected the reprogramming efficiency most (5-, 12-, and 3-fold reduction when *Elk1*-hRNA was transduced at D0, D4 and D8, respectively, Figure 6K; and 7-, 5-, and 1-fold reduction when *Gli2*-shRNA was transduced at D0, D4 and D8, respectively, Figure 6L). On the other hand, overexpression of *Elk1* or *Gli2* enhanced M9-mediated neural reprogramming (Figure S6E), validating that Elk1 and Gli2 are directly involved in M9-induced neural reprogramming.

To explore how mechanistically Elk1 and Gli2 participated in neural program induction, we hypothesized that they may directly bind and activate neural master genes in the presence of M9. Sox2 is such a master TF for neural fate specification *in vivo* (Graham et al., 2003; Thomson et al., 2011; Zhao et al., 2004), and it was reported that overexpression of Sox2 alone is able to convert mouse and human fibroblasts into NSCs *in vitro* (Ring et al., 2012). In M9-mediated neural reprogramming, Sox2 was gradually induced (Figure 5A and S5). To examine whether Elk1 and Gli2 directly bound to *Sox2* regulatory regions, ChIP-seq analysis revealed a dramatic increase of *Sox2* promoter binding by both Elk1 and Gli2 upon M9 treatment, confirming their regulatory role in activating *Sox2* transcription (Figure 6M). This was validated by ChIP-qPCR (Figure 6N, 6O and Table S6). Similarly, we also detected the binding of Elk1 and Gli2 at the promoter of *Ascl1*, another master neural fate TF (Figure S6F). Collectively, those data confirmed that M9 treatment leads to specific induction of master neural TFs, at least in part via direct binding to their regulatory regions by Elk1 and Gli2 (which are direct downstream effectors of the M9 treatment). Notably, this direct binding was transient, which peaked at day 4 and decreased at the late stage, indicating a critical time window in neural program induction (Figure 6M–O, and S6F). This mechanism is also supported by the observations that the transcriptional profile shifts and the epigenetic status switches towards NSC fate at the early stage of M9-induced neural reprogramming (Figure 5), and that the early-stage knockdown of *Elk1* and *Gli2* genes affect reprogramming efficiency most (Figure 6K and L). To further characterize their role in inducing neural program, we analyzed the genome localization of Elk1 and Gli2 upon M9 treatment by ChIP-seq. GO analysis revealed that Elk1 and Gli2 co-bind the regulatory regions of the genes that fall into categories of stem cell development and neural programs (Figure S6G), consistent with the mechanism by which they participate in neural induction. Remarkably, most of these genes (~60 %) showed increased H3K4me3 and decreased H3K27me3 (day 4 versus day 0) at their promoter region, suggesting that their binding may potentiate target gene activation. Collectively, our results suggest that M9 activates Elk1 and Gli2, which, in turn, directly bind to and activate neural genes, and consequently initiate the neural reprogramming cascade.

DISCUSSION

In this study, we identified and characterized a completely chemically defined condition using small molecules that enables efficient and specific reprogramming of mouse fibroblasts into ciNSLCs. The generated ciNSLCs resemble primary NSCs in several key aspects, including the similar molecular profiles, and the abilities to self-renew long-term and differentiate into functional neurons, astrocytes, and oligodendrocytes. Our in-depth functional studies demonstrating the post-synaptic potential for the ciNSLC-derived mature neurons and *in vivo* engraftment of ciNSLCs further establish the full potentials of ciNSLC and consequently authenticate the chemical reprogramming approach. In addition, our chemical condition specifically induced neural program than other lineages, validating its functional specificity. This neural reprogramming provides a unique process to investigate the mechanism underlying chemical-induced lineage-specific cell fate conversion.

Previous studies achieved neural reprogramming by introducing neural specific TFs (Han et al., 2012; Lujan et al., 2012). We previously devised the approach of cell-activation and signaling- directed (CASD) reprogramming, which entails transient overexpression of reprogramming inducing factors to dedifferentiate cells into an epigenetically activated state (cell activation, CA) in conjunction with lineage-specific signals (signaling-directed, SD) to reprogram fibroblasts into neural progenitor cells and other cell types (Kim et al., 2011; Zhang et al., 2014; Zhu et al., 2014). In both paradigms, the exogenously expressed TFs directly bind to specific loci across genome and recruit/cooperate with other transcriptional co-regulators (including epigenetic enzymes) to remodel the epigenome, and eventually establish the NSC fate. In contrast, chemical-mediated cellular reprogramming represents a distinct process and mechanism, in which the chemicals interact with the endogenous fibroblast-specific factors (without target neural cell type specificity in the first place) and indirectly rewire the transcriptional and epigenetic programs toward neural lineage. Our present study indicates that chemically defined conditions, such as our M9 condition, could achieve CASD process and induce intrinsic neural program. We provided an initial mechanistic entry into how specific TFs (e.g., Elk1 and Gli2) downstream of particular signaling pathways (e.g., bFGF and Shh) bind to endogenous master neural genes (e.g., *Sox2*) and participate in (in conjunction with other transcriptional and epigenetic remodeling) specifying the neural identity. Further study would be required to better characterize the specificity of the inductive cocktail, as well as the plasticity of the intermediate during this process.

Given the broad utility of the chemical reprogramming paradigm and an increasing number of small molecules identified for reprogramming and differentiation, our study may contribute to the development of potential treatments for neurodegenerative diseases and injuries, and provide routes for generating other lineage-specific cell types.

EXPERIMENTAL PROCEDURES

Chemical Conversion of Fibroblasts to ciNSLCs

Small molecules, including CHIR99021 (catalog number 4423), A83-01 (catalog number 2939), RG108 (catalog number 3295), Parnate (catalog number 3852), and SMER28

(catalog number 4297) from Tocris BioScience, Hh-Ag 1.5 from Excess Biosciences (catalog number M60004-2s), retinoic acid from Sigma (catalog number R2625), and LDN193189 from Cellagen Technology (catalog number C5361-2), were dissolved and diluted in DMSO. bFGF is from Peprotech (catalog number 100-18C), and was reconstituted in 1×PBS containing 0.05 % BSA and 4 mM HCl. tdMEFs were obtained by sorting for $p75^{-}$ /$tdTomato^{+}$ cells from MEFs derived from E13.5 mouse embryos of *Fsp1-Cre/ROSA26*^{tdTomato} background. To convert the mouse embryonic fibroblasts into ciNSLCs, tdMEFs were seeded into Matrigel (Corning, 1:40 dilution)-coated 24-well plates at 15,000 per well in MEF medium (Dulbecco's Modified Eagle Medium supplemented with 10% FBS, 0.1 mM nonessential amino acids, and 2 mM Glutamax). After an overnight culture, tdMEFs were washed twice with 1 ×PBS before being cultured in freshly prepared M9 medium (50% Neural basal, 50% DMEM/F12/Glutamax, 1 ×N2, 1 ×B27 without vitamin A, 0.075% BSA, 0.1 mM nonessential amino acids, with 3 μM CHIR99021, 100 nM LDN193189, 0.5 μM A83-01, 0.5 μM Hh-Ag1.5, 1 μM retinoic acid, 10 μM SMER28, 10 μM RG108, 2 μM Parnate, and 10 ng/ml bFGF) at 5% O_2 and 5% CO_2 incubator at 37°C. M9 medium was refreshed each other day. After a 10-day induction, cells were cultured in neural stem cells medium (NSC medium, 50% Neural basal, 50% DMEM/F12/Glutamax, 1 ×N2, 1 ×B27 without vitamin A, 0.075% BSA, 0.1mM nonessential amino acids, 20 ng/ml bFGF, and 20 ng/ml EGF). NSC medium was refreshed daily. Afterwards, the cells could be repeatedly propagated in NSC medium. Information about chemicals used in this study can be found in Table S3. Detail protocol can be found in "SUPPLEMENTAL EXPERIMENTAL PROCEDURES". Procedures involving mice were approved by the Institutional Animal Care and Use Committee at the University of California, San Francisco.

Supplementary Material

Refer to Web version on PubMed Central for supplementary material.

Acknowledgments

We thank Dr. Deepak Srivastava and Ms.Yu Huang at the Gladstone Institute of Cardiovascular Disease for providing Fsp1-Cre mice; Dr. Ken Nakamura at the Gladstone Institute of Neurological Disease for providing ROSA26^{tdTomato} mice; Drs. Li Gan and Yungui Zhou at the Gladstone Institute of Neurological Disease for providing the mouse cortical neurons; and Drs. Gary Howard and Crystal Herron at Gladstone Institutes for manuscript editing. We thank Alexander Williams and Sean Thomas at the Gladstone Bioinformatics Core for processing the sequencing data. S.D. was supported by funding from the California Institute for Regenerative Medicine, the Eunice Kennedy Shriver National Institute of Child Health and Human Development, the National Heart, Lung, and Blood Institute, the National Eye Institute/National Institutes of Health, the Roddenberry Foundation, the William K. Bowes, Jr. Foundation, and the Gladstone Institutes. Y.H. is supported by funding from the National Institute of Aging (AG048030) and the Roddenberry Foundation.

REFERENCES

Babu GJ, Lalli MJ, Sussman MA, Sadoshima J, Periasamy M. Phosphorylation of elk-1 by MEK/ERK pathway is necessary for c-fos gene activation during cardiac myocyte hypertrophy. J Mol Cell Cardiol. 2000; 32:1447–1457. [PubMed: 10900171]

Besnard A, Galan-Rodriguez B, Vanhoutte P, Caboche J. Elk-1 a transcription factor with multiple facets in the brain. Front Neurosci. 2011; 5:35. [PubMed: 21441990]

Cassady JP, D'Alessio AC, Sarkar S, Dani VS, Fan ZP, Ganz K, Roessler R, Sur M, Young RA, Jaenisch R. Direct lineage conversion of adult mouse liver cells and B lymphocytes to neural stem cells. Stem Cell Reports. 2014; 3:948–956. [PubMed: 25454632]

Chambers SM, Fasano CA, Papapetrou EP, Tomishima M, Sadelain M, Studer L. Highly efficient neural conversion of human ES and iPS cells by dual inhibition of SMAD signaling. Nat Biotechnol. 2009; 27:275–280. [PubMed: 19252484]

Cheng L, Hu W, Qiu B, Zhao J, Yu Y, Guan W, Wang M, Yang W, Pei G. Generation of neural progenitor cells by chemical cocktails and hypoxia. Cell Res. 2014; 25:645–646. [PubMed: 25941173]

Conti L, Pollard SM, Gorba T, Reitano E, Toselli M, Biella G, Sun Y, Sanzone S, Ying QL, Cattaneo E, et al. Niche-independent symmetrical self-renewal of a mammalian tissue stem cell. PLoS Biol. 2005; 3:e283. [PubMed: 16086633]

Cruzalegui FH, Cano E, Treisman R. ERK activation induces phosphorylation of Elk-1 at multiple S/T-P motifs to high stoichiometry. Oncogene. 1999; 18:7948–7957. [PubMed: 10637505]

Doetsch F, Caille I, Lim DA, Garcia-Verdugo JM, Alvarez-Buylla A. Subventricular zone astrocytes are neural stem cells in the adult mammalian brain. Cell. 1999; 97:703–716. [PubMed: 10380923]

Elkabetz Y, Panagiotakos G, Al Shamy G, Socci ND, Tabar V, Studer L. Human ES cell-derived neural rosettes reveal a functionally distinct early neural stem cell stage. Genes Dev. 2008; 22:152–165. [PubMed: 18198334]

Glaser T, Pollard SM, Smith A, Brustle O. Tripotential differentiation of adherently expandable neural stem (NS) cells. PLoS One. 2007; 2:e298. [PubMed: 17356704]

Graham V, Khudyakov J, Ellis P, Pevny L. SOX2 functions to maintain neural progenitor identity. Neuron. 2003; 39:749–765. [PubMed: 12948443]

Gritti A, Parati EA, Cova L, Forolichsthal P, Galli R, Wanke E, Faravelli L, Morassutti DJ, Roisen FNDD, Vescovi AL. Multipotential stem cells from the adult mouse brain proliferate and self-renew in response to basic fibroblast growth factor. J Neurosci. 1996; 16:1091–1100. [PubMed: 8558238]

Han DW, Tapia N, Hermann A, Hemmer K, Hoing S, Arauzo-Bravo MJ, Zaehres H, Wu G, Frank S, Moritz S, et al. Direct Reprogramming of Fibroblasts into Neural Stem Cells by Defined Factors. Cell Stem Cell. 2012; 10:465–472. [PubMed: 22445517]

Kim J, Efe JA, Zhu S, Talantova M, Yuan X, Wang S, Lipton SA, Zhang K, Ding S. Direct reprogramming of mouse fibroblasts to neural progenitors. Proc Natl Acad Sci U S A. 2011; 108:7838–7843. [PubMed: 21521790]

Koch P, Opitz T, Steinbeck JA, Ladewig J, Brustle O. A rosette-type, self-renewing human ES cell-derived neural stem cell with potential for in vitro instruction and synaptic integration. Proc Natl Acad Sci U S A. 2009; 106:3225–3230. [PubMed: 19218428]

Kondo T, Raff M. Oligodendrocyte precursor cells reprogrammed to become multipotential CNS stem cells. Science. 2000; 289:1754–1757. [PubMed: 10976069]

Lai K, Kaspar BK, Gage FH, Schaffer DV. Sonic hedgehog regulates adult neural porgenitor proliferation in vitro and in vivo. Nat Neurosci. 2003; 6:21–27. [PubMed: 12469128]

Lee J, Sayed N, Hunter A, Au KF, Wong WH, Mocarski ES, Pera RR, Yakubov E, Cooke JP. Activation of innate immunity is required for efficient nuclear reprogramming. Cell. 2012; 151:547–558. [PubMed: 23101625]

Li R, Liang J, Ni S, Zhou T, Qing X, Li H, He W, Chen J, Li F, Zhuang Q, et al. A mesenchymal-to-epithelial transition initiates and is required for the nuclear reprogramming of mouse fibroblasts. Cell Stem Cell. 2010; 7:51–63. [PubMed: 20621050]

Li W, Sun W, Zhang Y, Wei W, Ambasudhan R, Xia P, Talantova M, Lin T, Kim J, Wang X, et al. Rapid induction and long-term self-renewal of primitive neural precursors from human embryonic stem cells by small molecule inhibitors. Proc Natl Acad Sci U S A. 2011; 108:8299–8304. [PubMed: 21525408]

Lu J, Liu H, Huang CT, Chen H, Du Z, Liu Y, Sherafat MA, Zhang SC. Generation of integration-free and region-specific neural progenitors from primate fibroblasts. Cell Rep. 2013; 3:1580–1591. [PubMed: 23643533]

Lujan E, Chanda S, Ahlenius H, Sudhof TC, Wernig M. Direct conversion of mouse fibroblasts to self-renewing, tripotent neural precursor cells. Proc Natl Acad Sci U S A. 2012; 109:2527–2532. [PubMed: 22308465]

Machold R, Hayashi S, Rutlin M, Muzumdar M, Nery S, Corbin JG, Gritli-Linde A, Dellovade T, Porter JA, Rubin LL, et al. Sonic hedgehog is required for progenitor cell maintenance in telencephalic stem cell niches. Neuron. 2003; 39:937–950. [PubMed: 12971894]

Najm FJ, Lager AM, Zaremba A, Wyatt K, Caprariello AV, Factor DC, Karl RT, Maeda T, Miller RH, Tesar PJ. Transcription factor-mediated reprogramming of fibroblasts to expandable, myelinogenic oligodendrocyte progenitor cells. Nat Biotechnol. 2013; 31:426–433. [PubMed: 23584611]

Pan Y, Bai CB, Joyner AL, Wang B. Sonic hedgehog signaling regulates Gli2 transcriptional activity by suppressing its processing and degradation. Mol Cell Biol. 2006; 26:3365–3377. [PubMed: 16611981]

Pollard SM, Conti L, Sun Y, Goffredo D, Smith A. Adherent neural stem (NS) cells from fetal and adult forebrain. Cereb Cortex. 2006; 16(Suppl 1):i112–i120. [PubMed: 16766697]

Qian L, Huang Y, Spencer CI, Foley A, Vedantham V, Liu L, Conway SJ, Fu JD, Srivastava D. In vivo reprogramming of murine cardiac fibroblasts into induced cardiomyocytes. Nature. 2012; 485:593–598. [PubMed: 22522929]

Ring KL, Tong LM, Balestra ME, Javier R, Andrews-Zwilling Y, Li G, Walker D, Zhang WR, Kreitzer AC, Huang Y. Direct reprogramming of mouse and human fibroblasts into multipotent neural stem cells with a single factor. Cell Stem Cell. 2012; 11:100–109. [PubMed: 22683203]

Smith JR, Vallier L, Lupo G, Alexander M, Harris WA, Pedersen RA. Inhibition of Activin/Nodal signaling promotes specification of human embryonic stem cells into neuroectoderm. Dev Biol. 2008; 313:107–117. [PubMed: 18022151]

Smith WC, Harland RM. Expression cloning of noggin, a new dorsalizing factor localized to the Spemann organizer in Xenopus embryos. Cell. 1992; 70:829–840. [PubMed: 1339313]

Takanaga H, Tsuchida-Straeten N, Nishide K, Watanabe A, Aburatani H, Kondo T. Gli2 is a novel regulator of Sox2 expression in telencephalic neuroepithelial cells. Stem Cells. 2009; 27:165–174. [PubMed: 18927476]

Thier M, Worsdorfer P, Lakes YB, Gorris R, Herms S, Opitz T, Seiferling D, Quandel T, Hoffmann P, Nothen MM, et al. Direct Conversion of Fibroblasts into Stably Expandable Neural Stem Cells. Cell Stem Cell. 2012; 10:473–479. [PubMed: 22445518]

Thomson M, Liu SJ, Zou LN, Smith Z, Meissner A, Ramanathan S. Pluripotency factors in embryonic stem cells regulate differentiation into germ layers. Cell. 2011; 145:875–889. [PubMed: 21663792]

Wang L, Huang W, Su H, Xue Y, Su Z, Liao B, Wang H, Bao X, Qin D, He J, et al. Generation of integration-free neural progenitor cells from cells in human urine. Nat Methods. 2013; 10:84–89. [PubMed: 23223155]

Xu T, Zhang M, Laurent T, Xie M, Ding S. Chemical Approaches for Modulating Lineage-Specific Stem Cells and Progenitors. Stem Cells Translational Medicine. 2013; 2:355–361. [PubMed: 23580542]

Yang SH, Shore P, Willingham N, Lakey JH, Sharrocks AD. The mechanism of phosphorylation-inducible activation of the ETS-domain transcription factor Elk-1. EMBO J. 1999; 18:5666–5674. [PubMed: 10523309]

Zhang, M.; Li, K.; Xie, M.; Ding, S. Chemical Approaches to Controlling Cell Fate. In: Moody, S., editor. Principles of Developmental Genetics. 2nd. Cambridge, USA: Academic Press; 2014. p. 59-76.

Zhao S, Nichols J, Smith AG, Li M. SoxB transcription factors specify neuroectodermal lineage choice in ES cells. Mol Cell Neurosci. 2004; 27:332–342. [PubMed: 15519247]

Zhu S, Ambasudhan R, Sun W, Kim HJ, Talantova M, Wang X, Zhang M, Zhang Y, Laurent T, Parker J, et al. Small molecules enable OCT4-mediated direct reprogramming into expandable human neural stem cells. Cell Res. 2014; 24:126–129. [PubMed: 24296783]

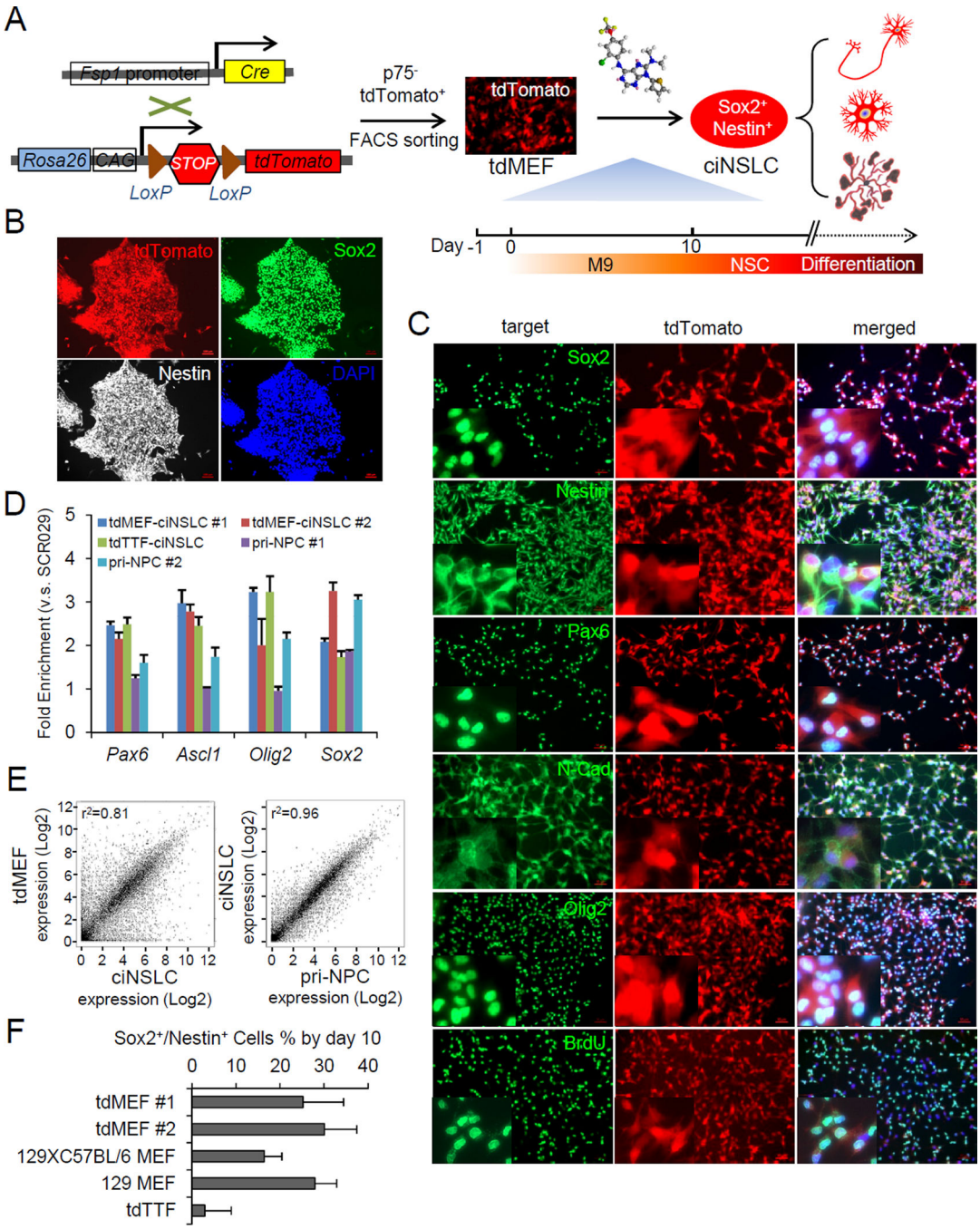

Figure 1. Conversion of MEF into ciNSLC by M9

(**A**) Schematic diagram illustrating the genetic lineage-tracing strategy (top panel) and the reprogramming protocol (bottom panel). tdMEFs were obtained by sorting for $p75^{-}$/$tdTomato^{+}$ cells from MEFs derived from E13.5 mouse embryos of *Fsp1-Cre/ROSA26*^{tdTomato} background.

(**B** and **C**) Immunostaining showing that tdMEF-derived ciNSLC colonies express Sox2 and Nestin (**B**), and that expanded ciNSLCs are positive for Sox2, Nestin, Pax6, N-Cadherin (N-

Cad), Olig2, and proliferate with incorporation of BrdU (**C**). Scale bar is 100 μm for (**B**) and 50 μm for (**C**).

(**D**) qRT-PCR analysis of the expression of indicated neural stem cell genes for two independent tdMEF-derived ciNSLC lines (tdMEF-ciNSLC #1 and #2), one tdTTF-derived ciNSLC line (tdTTF-ciNSLC), and two primary neural progenitor cell lines (pri-NPC #1 and #2). Gene expression (fold enrichment) was normalized to the control neural stem cell line SCR029.

(**E**) Paired scatter plot analysis comparing the global gene expression (Log2) of ciNSLC with tdMEF (left), and pri-NPC (right).

(**F**) Efficiency of M9-induced neural reprogramming was calculated for tdMEFs of different batches (tdMEF #1 and #2), 129×C57BL/6 MEFs, 129 MEFs, and tdTTFs (*Fsp1-Cre/ROSA26*^{tdTomato} genetically-traced mouse postnatal tail-tip fibroblasts), by calculating the percentage of Sox2^{+}/Nestin^{+} cells at day 10 after M9 treatment. Total cell number was determined by DAPI staining.

Data are represented as mean ± SEM. See also Figure S1–S3.

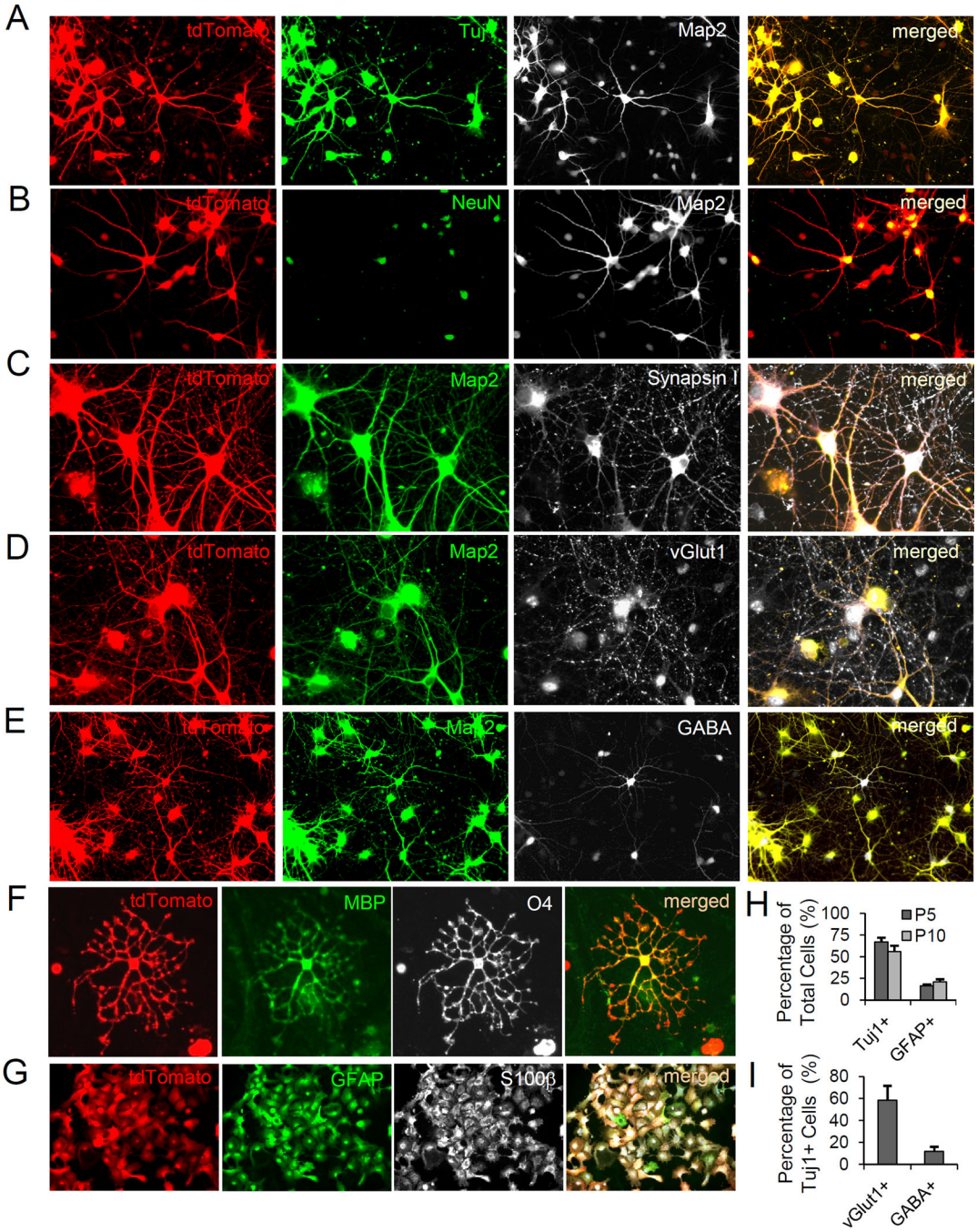

Figure 2. ciNSLCs Are Tripotent *in vitro*

(**A-G**) Immunostaining analysis showing that ciNSLCs differentiated into neurons that are positive for Map2 (**A-E**) and Tuj1(**A**), NeuN (**B**), Synapsin I (**C**), vGlut1 (**D**), and GABA (**E**), oligodendrocytes that are positive for O4 and MBP (**F**), and astrocytes that are positive for GFAP and S100β (**G**), respectively. Scale bar is 20 μm in (**A-E**), and 50 μm in (**F** and **G**). (**H**) Bar graph showing the percentage of neurons (Tuj1+) and astrocytes (GFAP+) in spontaneously differentiated ciNSLCs at passage 5 (P5) and passage 10 (P10). Total cell number was determined by staining with DAPI.

(**I**) Bar graph showing the percentage of vGlut1-positive glutamatergic neurons (vGlut1+) and GABA-positive GABAergic neurons (GABA+) out of total neurons. Total neurons were determined by staining for Tuj1.

Data are represented as mean ± SEM. See also Figure S4.

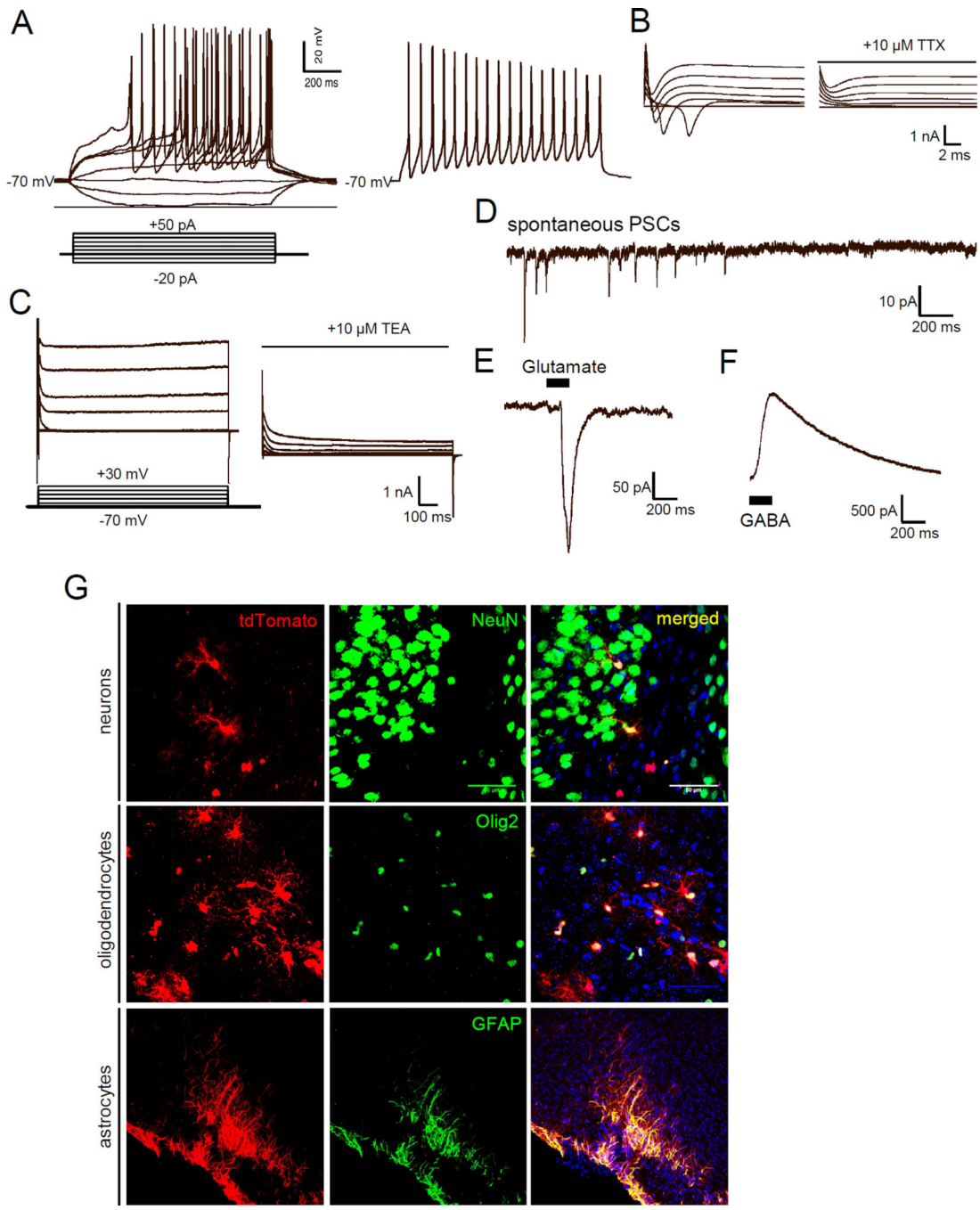

Figure 3. ciNSLC Generate Functional Neurons *in vitro* and Are Tripotent *in vivo*

(**A**) Representative traces of membrane potentials of ciNSLC-derived neurons in response to step-current injections (left), and current traces in response to 80 pA current injection (right). (**B** and **C**) Representative traces of whole-cell current in voltage-clamp mode. An inward current was observed and could be blocked by tetrodotoxin (TTX) (**B**), and an outward current could be blocked by tetraethylammonium (TEA) (**C**).

(**D**-**F**) Postsynaptic analysis of spontaneous synaptic network activities (PSCs) (**D**), excitatory postsynaptic currents in cells clamped at −70 mV in response to L-glutamate

puffs (**E**), and inhibitory postsynaptic currents in cells clamped at 0 mV in response to GABA puffs (**F**).

(**G**) Immunostaining analysis showing that tdTomato-labeled ciNSLCs differentiate into NeuN-positive neurons (top panel), Olig2-positive oligodendrocytes (middle panel), and GFAP-positive astrocytes (bottom panel) 4 weeks after injection into newborn mouse brain cortex. DAPI stains the brain section of injected site. Scale bar is 50 μm.

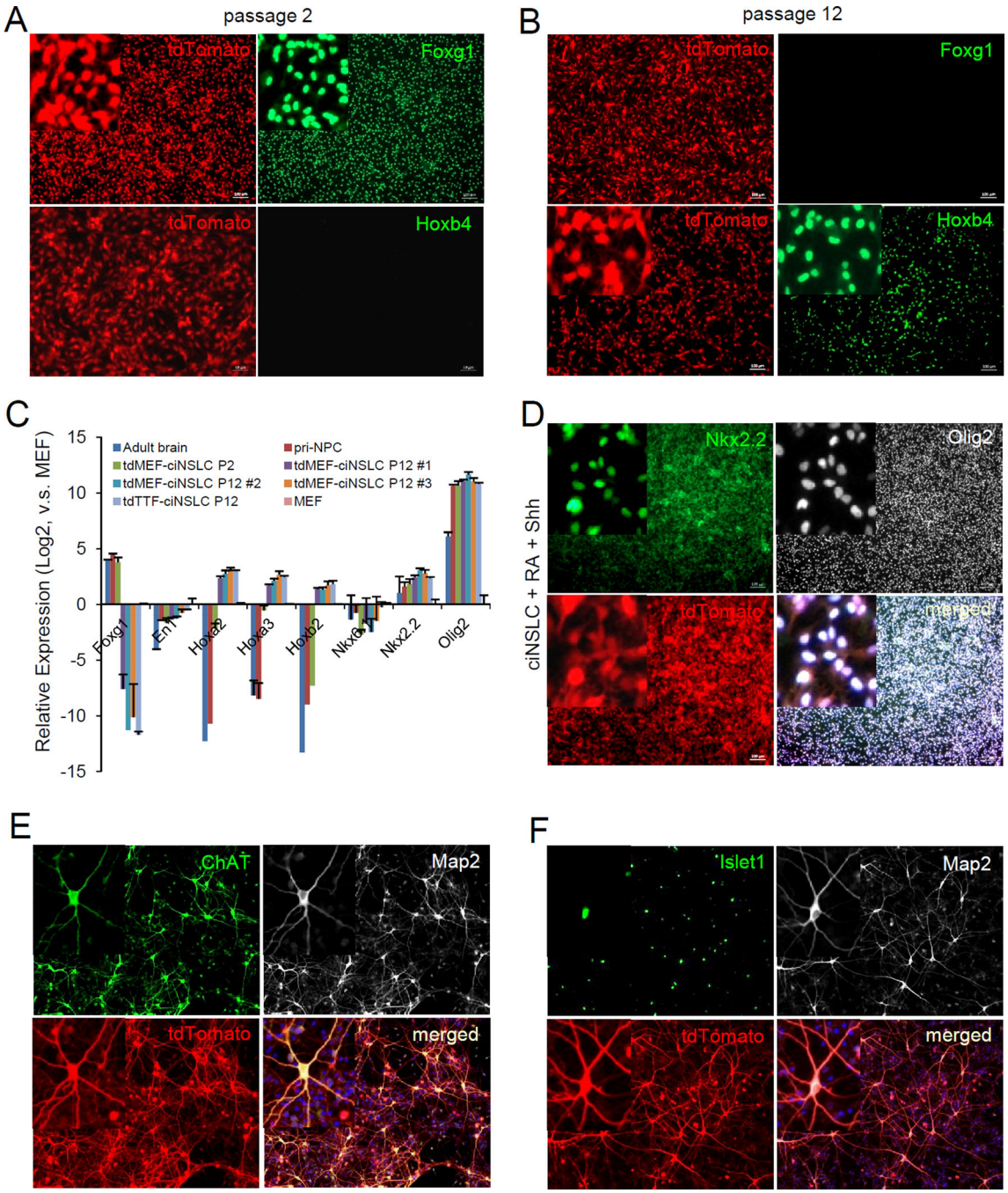

Figure 4. Characterization of Regional Property of Stable ciNSLCs

(**A, B** and **D**) Immunostaining analysis showing that passage 2 ciNSLCs are positive for Foxg1 and negative for Hoxb4 (**A**), passage 12 ciNSLCs are positive for Hoxb4 and negative for Foxg1 (**B**), and ciNSLCs after RA and Shh patterning are positive for Nkx2.2 and Olig2 (**D**). Scale bar is 50 μm for Hoxb4 in (**A**), and 100 μm for remaining images in (**A, B** and **D**). (**C**) qRT-PCR analysis showing the expression of indicated regional genes for tdMEF-derived ciNSLCs at passage 2 (tdMEF-ciNSLC P2) and passage 12 (three independent lines of tdMEF-ciNSLC P12 #1, #2 and #3), and tdTTF-derived ciNSLC at passage 12 (tdTTF-

ciNSLC P12). Gene expression (Log2) was normalized to that in tdMEFs (MEF). Adult mouse brain (Adult brain) and primary neural progenitor cells (pri-NPC) were used as controls. Data are represented as mean ± SEM.

(**E** and **F**) Immunostaining analysis showing that the RA/Shh-patterned ciNSLCs differentiated into neurons that are positive for Map2 and ChAT (**E**), and Islet1 (**F**). Scale bar is 50 μm. See also Figure S4.

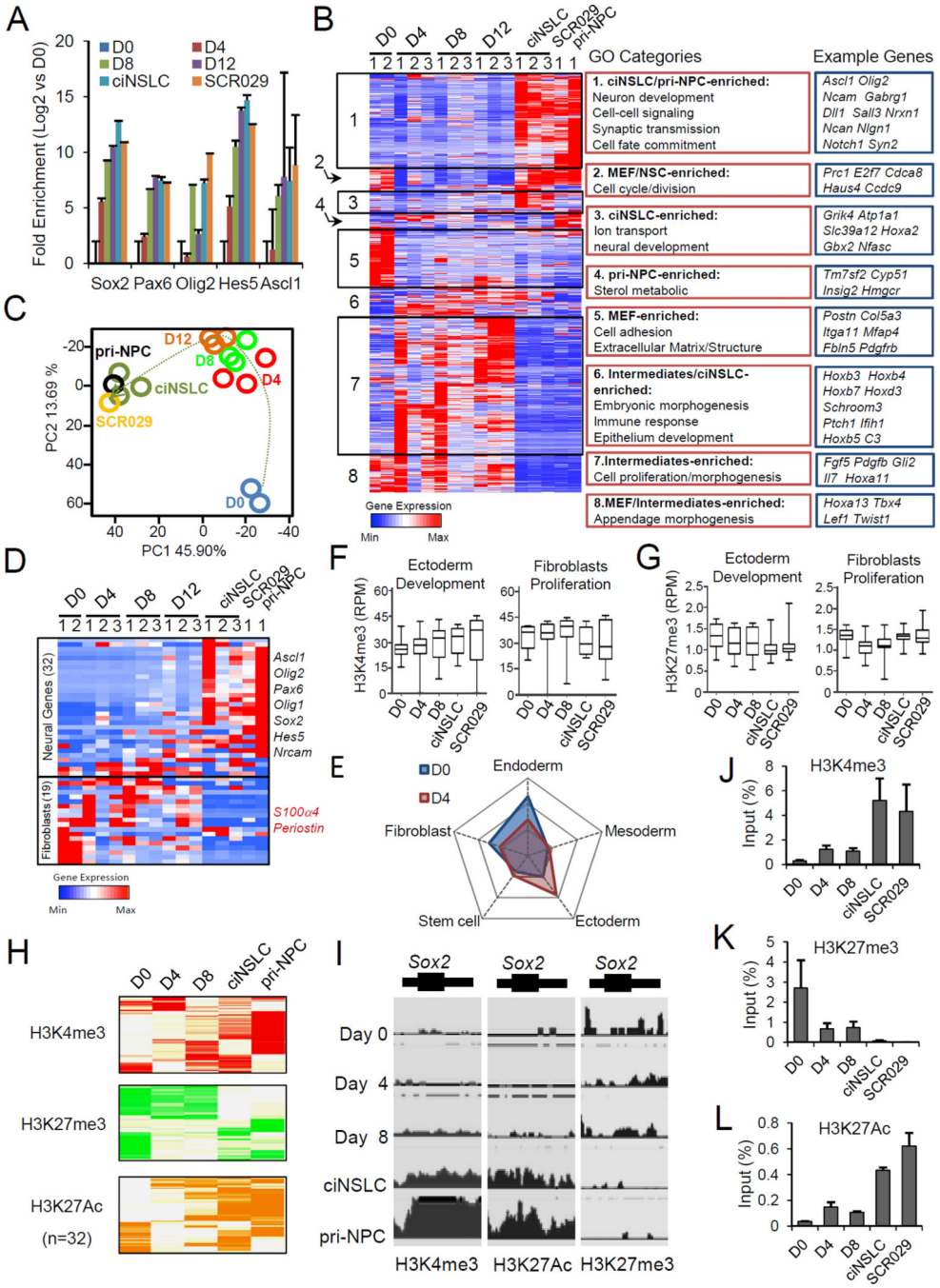

Figure 5. Molecular Roadmap of M9-Induced Neural Reprogramming

(**A**) qRT-PCR analysis showing the expression of neural genes at indicated time points. Gene expression (Log2) was normalized to that in tdMEFs.

(**B**) Heatmap (left) showing differentially expressed genes (*p* value<0.001) for samples of indicated time points (top left panel). The number above heatmap indicates independent biological replicates. Gene ontology (middle panel, red boxes) and example genes (right panel, blue boxes) for each block are shown (1 to 8, as labeled on left). Red and blue indicate upregulated and downregulated genes, respectively.

(**C**) Principle component analysis of samples from day 0 (D0), day 4 (D4), day 8 (D8), and day 12 (D12) of reprogramming, ciNSLCs, and the control neural stem cells pri-NPC and SCR029.

(**D**) Heatmap illustrating expression of the 32 neural stem cells-enriched genes and 19 fibroblasts-enriched genes for samples of indicated time points. The number above heatmap indicates independent biological replicates. Representative genes for each group are listed (right). Red and blue indicate upregulated and downregulated genes, respectively.

(**E**) Radar chart showing the average transcription activity of genes under GO terms of ectoderm, mesoderm, endoderm development, stem cell maintenance, and fibroblast proliferation, at day 0 (D0) and day 4 (D4) of reprogramming.

(**F** and **G**) Box plots showing the normalized intensity of H3K4me3 (**F**), and H3K27me3 (**G**) at promoter region of the genes under GO of ectoderm development, and fibroblasts proliferation, in indicated samples.

(**H**) Heatmap showing normalized intensity of histone modifications for 32 neural stem cell-enriched genes for indicated samples during neural reprogramming.

(**I**) Normalized ChIP-seq of histone modifications H3K4me3 (left), H3K27Ac (middle) and H3K27me3 (right) at *Sox2* genome loci in the indicated samples.

(**J**–**L**) ChIP-qPCR validating the histone modifications at *Sox2* promoter region for indicated samples. The relative abundance was normalized to Input.

Data are represented as mean ± SEM. See also Figure S5 and S6.

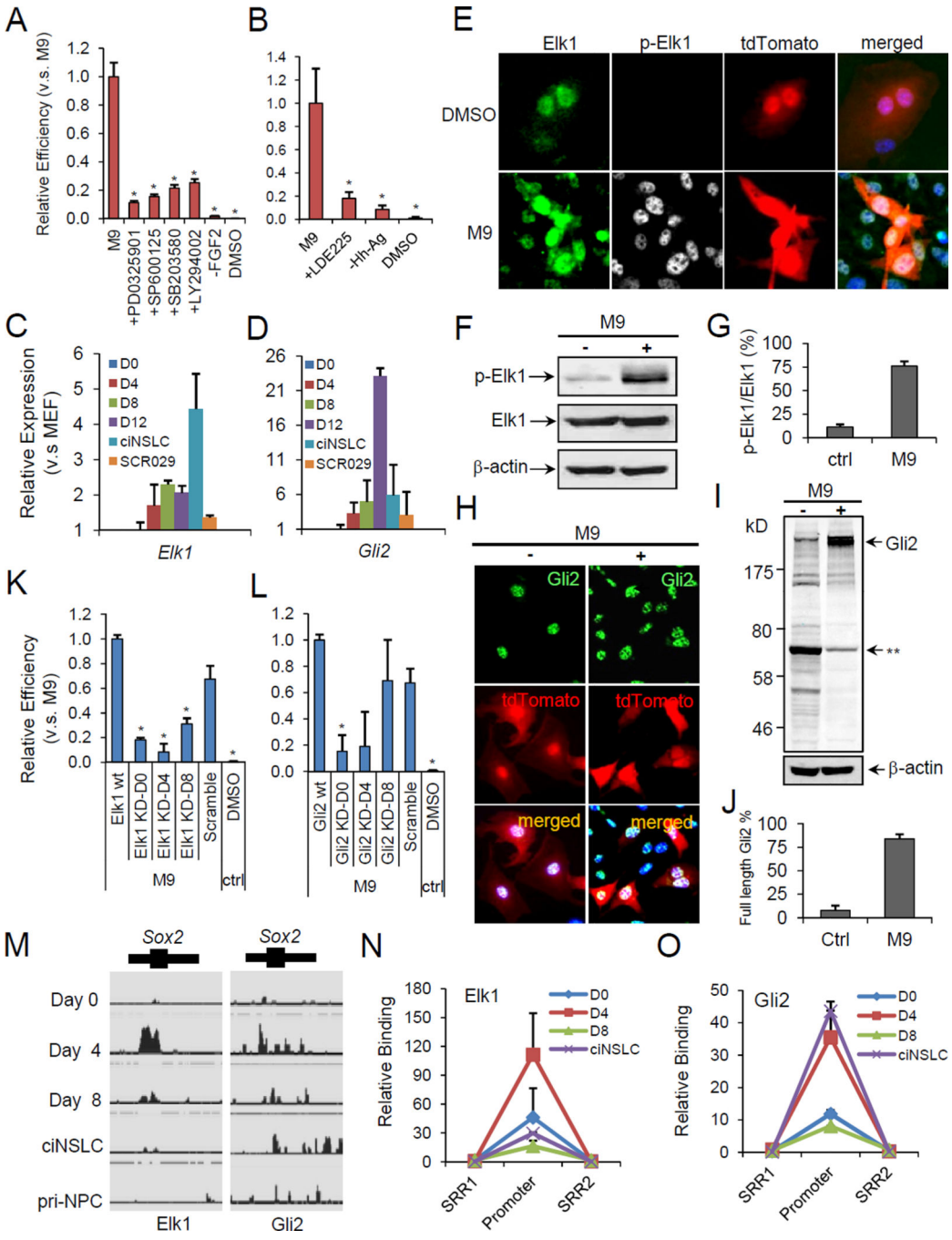

Figure 6. M9 Activates Intrinsic Neural Program

(**A, B, K** and **L**) Relative reprogramming efficiency 10 days after M9 treatment, with indicated small-molecule inhibitors (**A** and **B**), or when knocking down *Elk1* (**K**) or *Gli2* (**L**) at the indicated time points. The efficiency of M9-induced reprogramming at day 10 was assigned as "1". DMSO was negative control. "−" or "+" represents withdrawing or adding indicated component; wt, wild-type; KD, shRNA-mediated gene knockdown; **p* value <0.01.

(**C** and **D**) Expression of *Elk1* (**C**) and *Gli2* (**D**), monitored by qRT-PCR, for indicated samples during reprogramming. SCR029 served as control.

(**E–G**) Expression of Elk1 protein and its phosphorylation (p-Elk1) in unsorted MEFs were analyzed by immunostaining (**E**) and Western blot (**F**), 4 days after treatment with or without M9 (DMSO). The ratio of p-Elk1 over total Elk1 protein in (**F**) was calculated and normalized by the expression level of β-actin (**G**). Scale bar in (**E**) is 25 μm.

(**H–J**) Expression of Gli2 in unsorted MEFs 4 days after treatment in the absence (DMSO) or presence of M9 was analyzed by immunostaining (**H**) and Western blot (**I**). The percentage of full length Gli2 protein in (**I**) was calculated and normalized by the expression level of β-actin (**J**). Stars indicate degraded Gli2. Scale bar in (**H**) is 25 μm.

(**M**) Normalized ChIP-seq analysis showing the binding of Elk1 and Gli2 to *Sox2* genome loci at the indicated time points.

(**N** and **O**) ChIP-qPCR analysis showing the binding of Elk1 (**N**) or Gli2 (**O**) to *Sox2* regulatory regions, SRR1, SRR2, and promoter, at the indicated time points. Relative binding over IgG control is shown.

Data are represented as mean ± SEM. See also Figure S6.